Characterization of organic low-dielectric-constant materials using optical spectroscopy

K. Postava, T. Yamaguchi

Research Institute of Electronics, Shizuoka University, Johoku 3-5-1, Hamamatsu 432-8011, Japan

rpkamil@rie.shizuoka.ac.jp, rstyama@ipc.shizuoka.ac.jp

T. Nakano

Honeywell Electronic Materials Japan, Landic Minami-Azabu 4-11-21, Minato-ku, Tokyo 106-0047, Japan

Abstract: The dielectric function spectra of low dielectric constant (low-k) materials have been determined using high-precision four-zone null spectroscopic ellipsometry, near-normal incidence reflection spectrometry and Fourier transform infrared transmission spectroscopy. The optical functions over a wide spectral range from 0.03 to 5.4 eV (230 nm to 40.5 μm wavelength region) have been evaluated for representative low-k materials used in the semiconductor industry for interlayer dielectrics: (1) FLARE – organic spin-on polymer, and (2) HOSP – spin-on hybrid organic-siloxane polymer from the Honeywell Electronic Materials Company.

© 2001 Optical Society of America

OCIS codes: (310.6860) Thin films, optical properties; (160.4890) Organic materials; (260.2130) Ellipsometry and polarimetry; (300.6340) Spectroscopy, infrared

References and links

1. S.-W. Chung, J.-H. Shin, N.-H. Park and J. W. Park, "Dielectric properties of hydrogen silsesquioxane films degraded by heat and plasma treatment," Jpn. J. Appl. Phys., Part 1 **38**, 5214-5219 (1999).
2. S.-W. Chung, S.-T. Kim, J.-H. Shin, J. K. Kim and J. W. Park, "Comparative study of hydrido organo siloxane polymer and hydrogen silsesquioxane," Jpn. J. Appl. Phys., Part 1 **39**, 5809-5815 (2000).
3. J. J. Senkevich and S. B. Desu, "Poly(tetraflouro-p-xylylene), a low dielectric constant chemical vapor polymerized polymer," Appl. Phys. Lett. **72**, 258-260 (1998).
4. N. Aoi, "Novel porous films having low dielectric constants synthesized by liquid phase silylation of spin-on glass sol for intermetal dielectrics," Jpn. J. Appl. Phys., Part 1 **36**, 1355-1359 (1997).
5. T. Kikkawa, T. Nagahara and H. Matsuo, "Direct patterning of photosensitive low-dielectric-constant films using electron-beam lithography," Appl. Phys. Lett. **78**, 2557-2559 (2001).
6. S. M. Han and E. S. Aydil, "Reasons for lower dielectric constant of fluorinated SiO_2 films," J. Appl. Phys. **83**, 2172-2178 (1998).
7. K. Postava, T. Yamaguchi and M. Horie, "Estimation of the dielectric properties of low-k materials using optical spectroscopy," Appl. Phys. Lett. (2001) (to be published).
8. I. Ohlídal and D. Franta, Ellipsometry of thin film systems, in: *Progress in Optics* ed. E. Wolf (North-Holand, Amsterdam, 2000), Vol. 41.
9. K. Postava and T. Yamaguchi, "Optical functions of low-k materials for interlayer dielectrics," J. Appl. Phys. **89**, 2189-2193 (2001).
10. K. Postava, H. Sueki, M. Aoyama, T. Yamaguchi, Ch. Ino, Y. Igasaki and M. Horie, "Spectroscopic ellipsometry of epitaxial ZnO layer on sapphire substrate," J. Appl. Phys. **87**, 7820-7824 (2000).
11. K. Postava, M. Aoyama and T. Yamaguchi, "Optical characterization of TiN/SiO_2(1000 nm)/Si system by spectroscopic ellipsometry and reflectometry," Appl. Surf. Sci. **175-176**, 270-275 (2001).

#32940- $15.00 US

Received April 12, 2001; Revised July 26, 2001

(C) 2001 OSA

12. K. Postava, H. Sueki, M. Aoyama, T. Yamaguchi, K. Murakami and Y. Igasaki, "Doping effects on optical properties of epitaxial ZnO layers determined by spectroscopic ellipsometry," Appl. Surf. Sci. **175-176**, 543-548 (2001).
13. D. E. Aspens and A. A. Studna, "Dielectric functions and optical parameters of Si, Ge, GaP, GaAs, GaSb, InP, InAs, and InSb from 1.5 to 6.0 eV," Phys. Rev. B **27**, 985-1009 (1983).
14. D. F. Edwards, Silicon (Si), in: *Handbook of Optical Constants of Solids*, ed. E. D. Palik (Academic Press, New York 1998).
15. H. H. Willard, L. L. Merritt, Jr., J. A. Dean and F. A. Settle, Jr., *Instrumental Methods of Analysis*, 7th ed., Wadsworth Publishing Company, p. 287.
16. H.-U. Gremlich, Infrared and Raman Spectroscopy, in: *Ullmann's Encyclopedia of Industrial Chemistry*, Vol. B5, (Verlagsgesellschaft 1994).
17. G. E. Jellison, Jr. and F. A. Modine, "Parameterization of the optical functions of amorphous materials in the interband region," Appl. Phys. Lett. **69**, 371-373 and 2137 (1996).
18. H. R. Philipp, Silicon Dioxide (SiO_2) (Glass), in: *Handbook of Optical Constants of Solids*, ed. E. D. Palik (Academic Press, New York 1998).
19. G. Bader, P. V. Ashrit, F. E. Girouard and Vo-Van Truong, "Reflection–transmission photoellipsometry: theory and experiments," Appl. Opt. **34**, 1684-1691 (1995).
20. I. Ohlídal, "Approximate formulas for the reflectance, transmittance, and scattering losses of nonabsorbing multilayer systems with randomly rough boundaries," J. Opt. Soc. Am. A **10**, 158-171 (1993).

1 Introduction

Ultralarge scale integration (ULSI) of recent semiconductor high performance integrated circuits requires modern materials for interlayer and intermetal dielectrics. The standard insulating material, silicon dioxide, with a static dielectric constant of above 4 is unable to fulfill the requirements for ultra large scale integration. Therefore, low dielectric constant (low-k) materials have recently been developed using new organic polymers which present great possibility for dielectric and thermal property adjustment [1-5].

Accurate data on the optical properties of low-k materials over a wide spectral range are essential for: (1) thickness control using spectroscopic micro-reflectometry in real time, (2) evaluation of electronic and ionic contributions to the static dielectric constant [6, 7] and (3) possibility estimation of lower the material dielectric constant. Optical functions of thin films are usually determined using spectroscopic ellipsometry [8], which measures two independent quantities (ellipsometric angles ψ and Δ) related to each other by Kramers-Kronig dispersion relations. In our previous paper [9], the optical functions of SiLK (semiconductor dielectric resin from the Dow Chemical Company) and Nanoglass (nanoporous silica from the Honeywell Electronic Materials Company) were obtained in the spectral range from 0.5 to 5.4 eV using a simultaneous treatment of ellipsometric and reflectivity data.

This paper deals with two another candidates of low-k materials prepared by spin-on coating. The first is an organic polymer FLARE from Honeywell Advanced Microelectronic Materials. FLARE is an bridged poly-arylene ether with a dielectric constant of 2.8 and thermal stability of up to 400°C. The second material, HOSP from Honeywell Advanced Microelectronic Materials, is a spin-on hybrid siloxane-organic polymer with a dielectric constant of 2.5 and thermal stability of up to 550°C. Both materials are compatible with both multi-level copper damascene structures and traditional aluminum/tungsten interconnect technologies. The ellipsometric and reflectivity measurements covering the ultraviolet, visible and near infrared region were, in addition, completed with Fourier transform infrared transmission spectroscopy. Consequently, the optical functions of FLARE and HOSP were obtained over a wide spectral range from 0.03 to 5.4 eV (230 nm to 40.5 μm wavelength region). Sample preparation and experimental procedures are described in Sec. 2. The experimental results obtained for FLARE and HOSP materials and the optical functions obtained are presented in Sec. 3.

#32940- $15.00 US Received April 12, 2001; Revised July 26, 2001
(C) 2001 OSA

2 Experimental

2.1 *Sample preparation*

The low-k layers were prepared on 0.72 mm thick single-crystal silicon wafers. The wafers were coated using a SEMIX TR8132-C coater and the thicknesses of the FLARE and HOSP layers were approximately 400 nm. To achieve optimal chemical, mechanical and electrical properties, films have to be thermally cured at high temperatures. During the thermal cure process, chemical bounds are formed in the polymer which create an isotropic network structure that provides mechanical strength, solvent resistance, and high thermal stability. The wafers were baked and cured under nitrogen ambient. Table 1 shows the bake plate and cure conditions for FLARE and HOSP layers.

Table 1. Bake plate and cure conditions for FLARE and HOSP

Procedure	Temperature	Time (min)
Bake		
Hot plate 1	150°C	1
Hot plate 2	200°C	1
Hot plate 3	250°C (FLARE) 350°C (HOSP)	1
Cure		
Load wafers	200°C	1
Ramp rate	to 250°C	5°C/min
Dwell	250°C	10
Ramp rate	to 400°C	5°C/min
Dwell	400°C	60
Ramp rate	to 200°C	1.5°C/min
Remove wafers	200°C	1

2.2 *Spectroscopic ellipsometry and reflectometry*

A computer controlled four-zone null ellipsometer with PSCA (Polarizer—Sample—Compensator—Analyzer) configuration was employed in the spectral region from 1.5 to 5.4 eV (230–840 nm wavelength region). The four-zone averaging for two compensator azimuth angles ±45°, gives high precision measurements insensitive to the compensator, polarizer and analyzer azimuth angle errors and imperfections. Absence of systematic errors is essential for a reasonable determination of the unknown parameters. The measurements were performed under angles of incidence ranging from 60° to 80° in steps of 5° for HOSP, and 70°, 75° and 80° for FLARE, respectively. Other experimental details were described in Ref. [10].

The ellipsometric measurements were completed with near-normal incidence reflectometry in the spectral range from 0.5 to 6.5 eV (190 nm to 2.5 μm wavelength region). The simultaneous fit of the ellipsometric and reflectivity data decreases correlation between layer thickness and parameters describing layer optical functions [11, 12]. The measured reflectivity spectra were obtained using a double beam spectrometer (Shimadzu, UV–3100 PC). Since reflectometry is an intensity measurement, a calibration procedure is needed. We used a silicon wafer as a reference for the calibration. The measured data were fitted using the Levenberg-Marquardt least square algorithm.

#32940- $15.00 US
Received April 12, 2001; Revised July 26, 2001
(C) 2001 OSA

2.3 *Infrared transmission spectrometry*

The measured normal incidence transmission spectra were obtained using a Fourier-transform infrared spectrometer (JEOL, JIR-WINSPEC 50) in the spectral region from 0.03 to 0.52 eV (247–4194 cm^{-1} wavenumber region). In this study, we used a relative transmittance given by the ratio $T_{low-k/Si}/T_{Si}$, where T_{Si} is the transmittance of the silicon substrate and $T_{low-k/Si}$ is the transmittance of the silicon substrate coated by the low-k layer. The transmission is influenced by both the real ε_1 and imaginary ε_2 parts of the complex dielectric function, which relate to each other by Kramers–Kronig dispersion relations. The dielelectric function was parameterized using the function

$$\varepsilon(E) = \varepsilon_{1\infty} + \frac{AE_1^2}{E_1^2 - E^2} + \sum_n \frac{A_n E_{0n}^2}{E_{0n}^2 - E^2 + i\Gamma_n E_{0n} E}, \qquad (1)$$

where the first term $\varepsilon_{1\infty}$ and the second Sellmeier term describe a dispersion in the visible and near-infrared region. A and E_1 denote the amplitude and the energy of the absorption peak outside the measured range. The sum of damped harmonic oscillators corresponds to the infrared absorption structure. For example, the n-th absorption peak is described using the amplitude A_n, the Lorenz resonant frequency E_{0n} and the broadening parameter Γ_n. The model dielectric function (1) gives the simple static limit $\varepsilon(E \to 0) = \varepsilon_{1\infty} + A + \sum_n A_n,$, which enables the electronic (ultraviolet) $(\varepsilon_{1\infty} + A - 1)$ and the ionic (infrared) contributions to the static dielectric constant to be estimated [7]. The measured relative transmittance data were fitted using the dielectric function parameterization (1) to a model including incoherent propagation in the thick silicon substrate as discussed in Appendix.

3 Results

3.1 *FLARE*

Figure 1 shows the measured ellipsometric and reflectivity spectra the for FLARE layer. The spectra show strong oscillations originating from interference effects in the FLARE layer for energies smaller than ≈ 3 eV. In this visible and near infrared region, the layer is transparent. However, the oscillations are attenuated in the ultraviolet region and, in general, organic polymers are characterized by complicated optical functions.

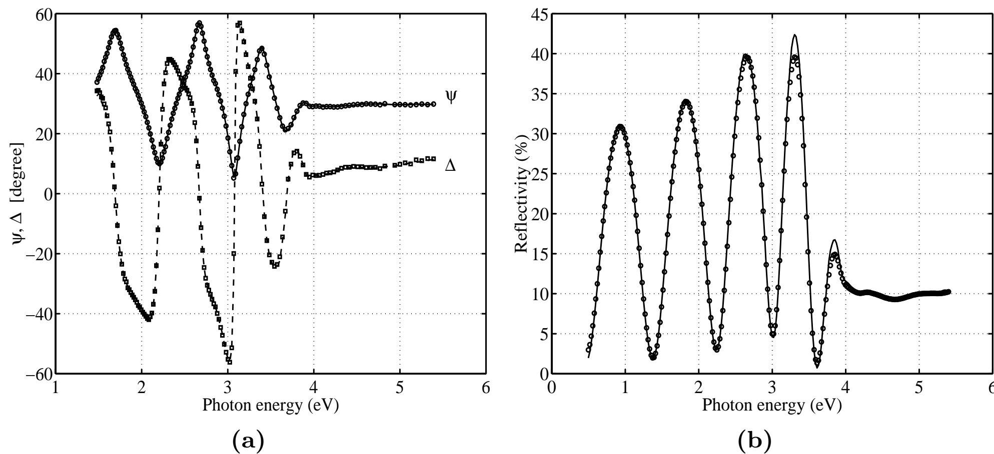

Fig. 1. Spectroellipsometric data at the incidence angle of 80° (a) and near-normal incidence reflectivity spectra (b) of FLARE layer. Measured data (circles, squares) are compared with the model (solid line).

#32940- $15.00 US
Received April 12, 2001; Revised July 26, 2001
(C) 2001 OSA

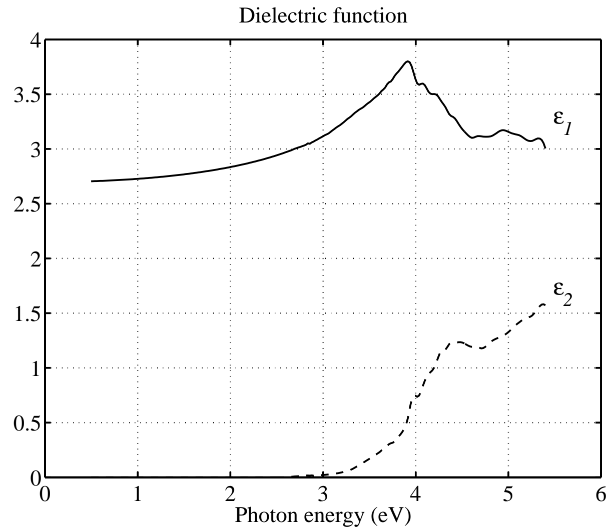

Fig. 2. Optical functions of FLARE in visible, near-infrared and near-ultraviolet range. Real part ε_1 and imaginary part ε_2 of the dielectric function are represented by solid and dashed lines.

The dielectric function parameterization of organic materials usually requires the many-oscillator model and includes many parameters which can be dependent. Consequently, we have determined the optical functions of FLARE using the two following steps:

1. Fitting the measured spectra in the transparent region using simple parameterization of the optical functions. The fit results to structural parameters, i. e., to a layer thickness.

2. Provided that the thickness is correctly determined, the optical constants (the refractive index and absorption coefficient) can be directly obtained from measured ellipsometric angles (ψ and Δ) separately for each wavelength.

In the case of FLARE, the dielectric function in the transparent region below 2.8 eV was parameterized using the non-dispersive and Sellmeier terms (Eq. (1)). The ellipsometric and reflectivity data were fitted simultaneously to a three-medium model, consisting of air/FLARE/Si. The layer thickness t, non-dispersive term $\varepsilon_{1\infty}$, the amplitude A and the energy E_1 were fitted parameters. The optical functions of the single-crystal Si substrate were taken from Refs. [13, 14]. The parameters obtained are listed in Table 2. In the second step, we calculated the FLARE optical functions directly from measured ellipsometric angles separately for each wavelength. Figure 2 shows the resulting dielectric function. Figure 1 shows a comparison between the model including the obtained optical functions and the measured data.

Figure 3 shows the measured relative transmission infrared spectra. The measured data were fitted to the model including incoherent summation in the thick silicon substrate. The optical functions of FLARE layer were parametrized using Eq. (1). The parameters $\varepsilon_{1\infty}$, A, E_1 and the thickness t were taken from the previous fit of ellipsometric and reflectivity data in the visible and near-infrared region. Absorptions in the infrared region were parameterized using 15 damped harmonic oscillators. The parameters A_n, E_{0n} and Γ_n obtained are listed in Table 2 and Figure 4 shows the corresponding dielectric function $\varepsilon = \varepsilon_1 - i\varepsilon_2$. The infrared spectrum of a compound is essentially the superposition of absorption bands of specific functional groups. The first

Table 2. Results of fit for the FLARE layer.

FLARE		$t = 407.0$ nm		
• visible, uv region – electronic contribution				
	$\varepsilon_{1\infty} = 2.074$		$(E < 2.8$ eV)	
	$A = 0.624$		$E_1 = 4.71$ eV	
• infrared region – ionic contribution				
n	A_n	E_{0n} (eV)	E_{0n} (cm^{-1})	Γ_n
1	0.00038	0.3784	3052	0.01452
2	0.00194	0.2065	1665	0.01084
3	0.00299	0.1974	1592	0.00859
4	0.00691	0.1857	1498	0.00848
5	0.00099	0.1802	1454	0.00468
6	0.00121	0.1759	1418	0.00421
7	0.00352	0.1597	1288	0.02499
8	0.02210	0.1537	1240	0.02085
9	0.00435	0.1448	1168	0.01009
10	0.00349	0.1370	1105	0.01860
11	0.00088	0.1257	1014	0.00516
12	0.00561	0.1079	871	0.03169
13	0.00635	0.1030	831	0.03074
14	0.01190	0.0924	745	0.02453
15	0.00641	0.0760	613	0.01909

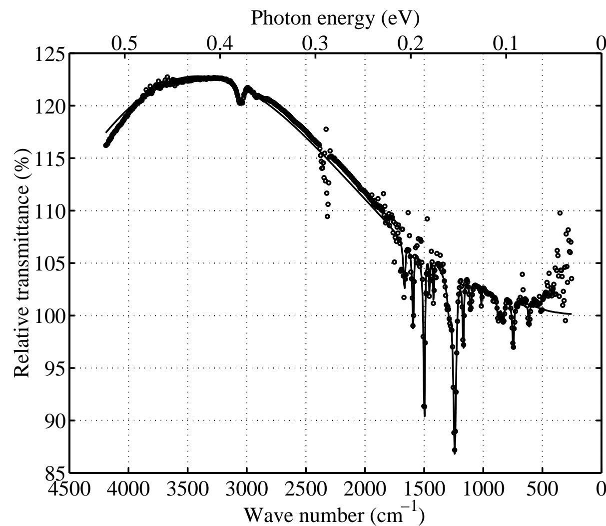

Fig. 3. Normal incidence relative transmission spectra of FLARE layer. Measured data (circles) are compared with the model (solid line).

Received April 12, 2001; Revised July 26, 2001

(C) 2001 OSA

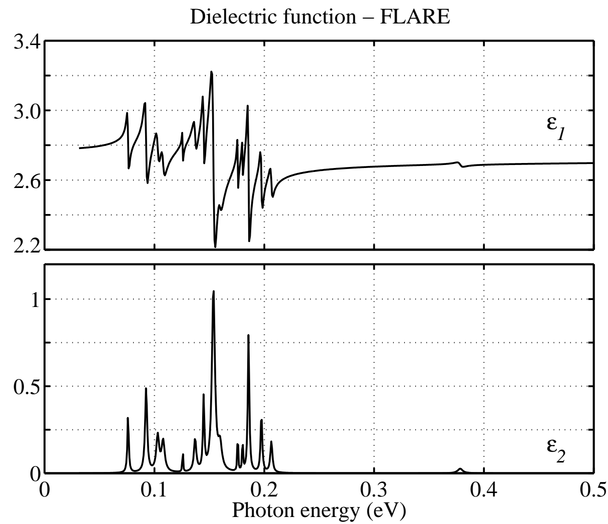

Fig. 4. Optical functions of FLARE in infrared spectral range.

FLARE absorption peak (n=1, Table 2) originates from hydrogen stretching vibrations (C − H), characteristic for aromatic and unsaturated compounds. The intermediate frequency range, 1300–1700 cm^{-1}, is often called the unsaturated region. The absorption peaks $n = 2 - 6$ correspond to the C = O, C = C aromatic and C − H alicyclic bounds. Relatively strong absorptions $n = 7, 8$ originate from C − O − C aromatic and aliphatic etheric stretches. The absorption peaks $n = 12-14$ correspond to C − O epoxide stretch.

3.2 *HOSP*

Figure 5 shows the measured ellipsometric and reflectivity spectra for the HOSP layer. The ellipsometric spectra (incidence angles ranging from 60° to 80° in steps of 5°) were treated simultaneously with near-normal incidence reflectivity data.

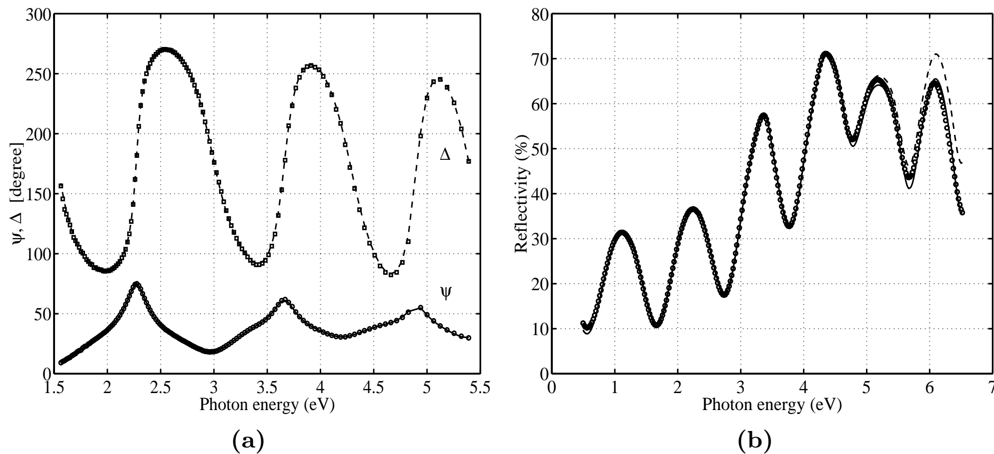

Fig. 5. Spectroellipsometric data at the incidence angle of 70° (a) and near-normal incidence reflectivity spectra (b) of HOSP layer. Measured ellipsometric angles ψ (circles) and Δ (squares) are compared with the model (solid line). Measured reflectivity data (circles) are compared with the model based on Tauc-Lorentz (solid line) and Sellmeier parameterization (dashed line), respectively.

#32940- $15.00 US
Received April 12, 2001; Revised July 26, 2001
(C) 2001 OSA

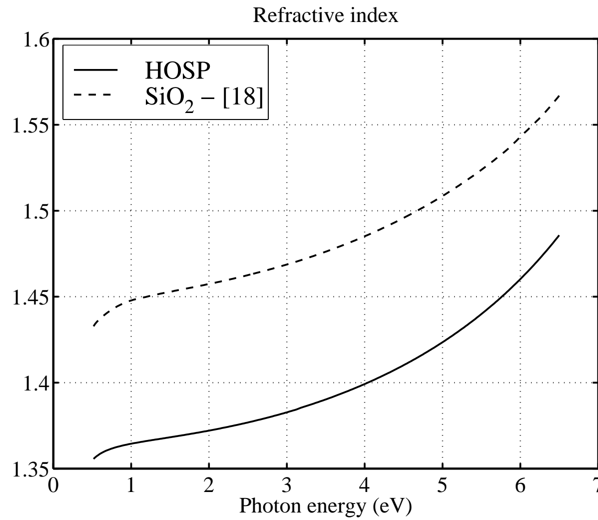

Fig. 6. Refractive index spectrum of HOSP (solid line) is compared with SiO_2 tabulated values (dashed line).

A simple model based on Sellmeir parameterization gave good fit to the ellipsometric data. The parameters obtained are listed in Table 3. However, this simple model gave a poor fit in the high energy reflectivity region (Fig. 5b, dashed line). The measured reflectivity shows a decrease and oscillation attenuation in the high energy region originating from a high energy absorption tail. We have included the high energy absorption tail using a Tauc-Lorentz parameterization instead of the simple Sellmeier function. Tauc-Lorentz parameterization was recently derived by Jellison and Modine [17] for the optical functions of amorphous materials. This formulation uses a combination of the Tauc band edge and the Lorentz oscillator function. The imaginary part of the complex dielectric function is given by

$$\begin{aligned} \varepsilon_2(E) &= \frac{AE_0C(E-E_g)^2}{(E^2-E_0^2)^2+C^2E^2}\frac{1}{E} \qquad && [E > E_g] \\ &= 0 && [E \leq E_g] \end{aligned} \tag{2}$$

The real part of the dielectric function is determined in a closed form from $\varepsilon_2(E)$ using Kramers-Kronig integration [17]. The model dielectric function employs five fitting parameters: the non-dispersive term $\varepsilon_{1\infty} = 1$, the band gap energy E_g, the amplitude A, the Lorenz resonant frequency E_0 and the broadening parameter C. The resulting parameters are $\varepsilon_{1\infty} = 1.32$, $E_g = 3.13$ eV, $A = 11.65$ eV, $E_0 = 10.48$ eV and $C = 0.205$ eV. The model including the improvement gives good agreement with the data (Figure 5, solid lines). Figure 6 shows the obtained refractive index n.

#32940- $15.00 US Received April 12, 2001; Revised July 26, 2001
(C) 2001 OSA

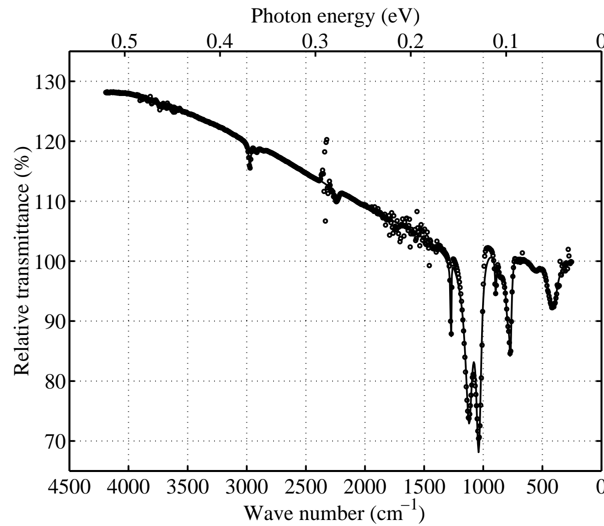

Fig. 7. Normal incidence relative transmission spectra of HOSP layer. Measured data (circles) are compared with the model (solid line).

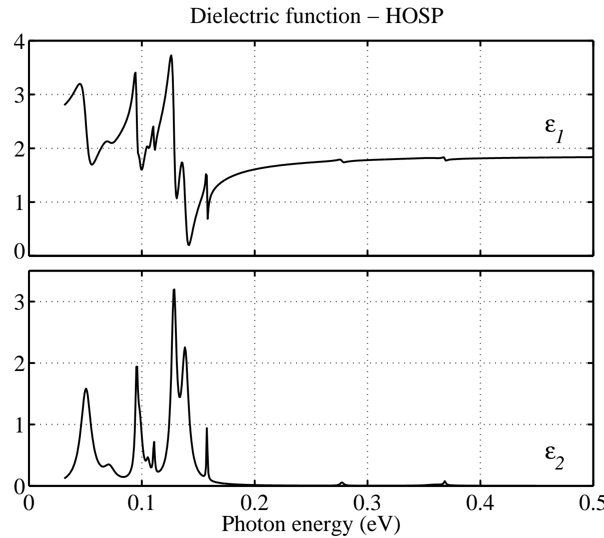

Fig. 8. Optical functions of HOSP in infrared spectral range.

Figure 7 shows the measured relative transmission spectra in the infrared region. The measured data were fitted to the model including incoherent summation in the thick silicon substrate. The optical functions of HOSP layer were parametrized using Eq. (1). The parameters $\varepsilon_{1\infty}$, A, E_1 and the thickness t were taken from the previous fit of ellipsometric and reflectivity data in the visible and near-infrared region. Absorptions in the infrared region were parameterized using 12 damped harmonic oscillators. The parameters A_n, E_{0n} and Γ_n obtained are listed in Table 3 and Figure 8 shows the corresponding dielectric function. The HOSP absorption peaks ($n = 1, 2$, Table 3) originate from hydrogen stretching vibrations ($\mathrm{C-H}$), characteristic for aliphatic (CH_3) com-

Table 3. Results of fit for the HOSP layer.

HOSP		$t = 407.3$ nm		
• visible, uv region – electronic contribution				
	$\varepsilon_{1\infty} = 1.315$		$(E < 5.5$ eV$)$	
	$A = 0.549$		$E_1 = 10.46$ eV	
• infrared region – ionic contribution				
n	A_n	E_{0n}		Γ_n
		(eV)	(cm^{-1})	
1	0.00034	0.3685	2972	0.00548
2	0.00121	0.3615	2915	0.06021
3	0.00072	0.2773	2236	0.01341
4	0.00561	0.1578	1272	0.00576
5	0.10988	0.1384	1117	0.05408
6	0.12509	0.1285	1037	0.04215
7	0.00791	0.1108	893	0.01415
8	0.00883	0.1055	851	0.03568
9	0.04359	0.0983	793	0.05222
10	0.04469	0.0954	770	0.02818
11	0.03584	0.0715	576	0.16202
12	0.33734	0.0508	410	0.21713

pounds. The absorption peaks $n = 3$ and $n = 4$ correspond to the Si – H and Si – C bounds, respectively. Strong absorptions $n = 5, 6$ originate from cage and normal Si – O stretches. The absorption peaks $n = 9, 10$ correspond to Si – O epoxide and Si – CH_3 stretches.

4 Conclusion

We have determined the optical functions of FLARE and HOSP in the spectral range from 0.03 to 5.4 eV. The method of optical function evaluation of the organic low-k materials over a wide spectral range, covering the ultraviolet, visible near- and mid-infrared regions (230 nm to 40.5 μm wavelength region) were demonstrated. A good agreement between the model and the measured data were obtained.

Appendix

In this appendix we describe how the incoherent reflections in a thick substrate affect the infrared transmittance. In terms of the amplitude reflection and transmission coefficients r_j and t_j $(j = s, p)$, the transmittance for a thick isotropic substrate is in the form [19]

$$T_j = \frac{\left|t_j^{(01)}\right|^2 \left|t_j^{(12)}\right|^2 e^{2\Im(k_z)d}}{1 - \left|r_j^{(10)}\right|^2 \left|r_j^{(12)}\right|^2 e^{4\Im(k_z)d}}, \quad j = s,\, p, \tag{3}$$

where d and $\Im(k_z)$ denote the substrate thickness and the imaginary part of the z-component of the wavevector. The upper indices represent a particular pseudointerface for which the coefficient is defined. Optical effects of the low-k thin film are included in the coefficients $t_j^{(01)}$ and $r_j^{(10)}$. For normal incidence we can omit the lower index j, because $T_s = T_p$. Figure 9 shows how the incoherent reflections affect the absolute $T_{\mathrm{low}-k/\mathrm{Si}}$

#32940- $15.00 US
Received April 12, 2001; Revised July 26, 2001
(C) 2001 OSA

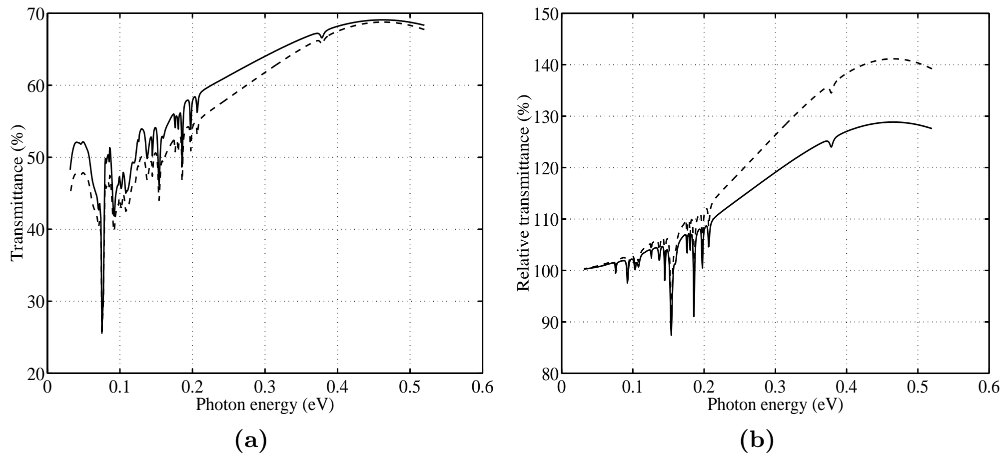

Fig. 9. Influence of incoherent reflections in the thick silicon substrate on the absolute (a) and relative (b) transmittance. The model including the incoherent reflections (solid lines) is compared with a simple transmission simulation neglecting this effect (dashed lines).

and relative $T_{\text{low}-k/\text{Si}}/T_{\text{Si}}$ transmittance using an example of FLARE low-k layer on thick Si substrate. The model based on Eq. (3) (solid line) is compared with the model neglecting the incoherent reflections in the thick substrate: $T_j = |t_j^{(01)}|^2|t_j^{(12)}|^2 e^{2\Im(k_z)d}$. Smooth interfaces and surfaces were considered in the simulation. The absolute transmittance (Fig. 9a) is significantly influenced by the incoherent reflections. Small difference between curves near maximum (≈ 0.45 eV) corresponds to anti-reflection behavior of low-k layer. The absolute transmittance is strongly sensitive to the absorption of thick silicon substrate, therefore measurements of the relative transmittance were taken.

This paragraph deals with back-side boundary roughness of Si substrate. Although an optimal transmittance measurement is taken on a both-side-polished wafer, the back-side silicon boundaries of our samples were rough. The roughness were included into data fitting using a simple model based on the scalar diffraction theory [20]. The approximative model provides a good agreement with relative transmittance data.

Received April 12, 2001; Revised July 26, 2001